Steering Angle Control of Front Wheel Independent Steering System for Cornering Maneuverability Enhancement

Junnian WANG [1)] Ruihao FAN [1)*] Zidong ZHOU [1)] Zhenyu WANG [1)] Fang Yang [2)]

1) State Key Laboratory of Automotive Simulation and Control, Jilin University, China

E-mail: wjn@jlu.edu.cn; aizaishenghua@sina.com

2) New Energy Development Institute of China FAW Group Co., Ltd., China

E-mail: yangfang1@faw.com.cn

ABSTRACT: At present, steer-by-wire technology has become one of the core members of active chassis technology, due to its benefit for ensuring active safety and handling performance of vehicle, especially for intelligent electric vehicles. In order to improve the maneuverability of the vehicle under extreme condition by steer-by-wire technology, a multi-mode steer-by-wire system is proposed in this paper. The structural composition and dynamic modeling of the proposed steering system is introduced first, then corresponding steering angle decision and following control strategy are described. Simulation results verified the feasibility and steering-angle control effect of the proposed multi-mode steer-by-wire system.

KEY WORDS: active chassis, steer-by-wire, vehicle stability, side-slip control, cornering performance

1. INTRODUCTION

As we know, in the case of steering, the lateral acceleration results in the normal load transfer from the inner wheel to the outer wheel, which causes the difference of the side-slip stiffness of the two wheels. In the severe cornering condition with large lateral acceleration, the lateral force of the inner wheel may be saturated. As for traditional steer-by-wire system, the relationship between the two front wheel steering angles are constrained by the steering trapezium. If the steering wheel angle is further increased when the tire lateral force is saturated, the lateral force of inner wheel will decrease with the increase of the side-slip angle. This phenomenon may increase the of load outer wheel and even push it into its saturation zone. Moreover, the limit cornering ability of the vehicle is mitigated and even the car may lose stability.

Active independent front wheel steering system (AIFS) first proposed by Ahmed et al,[1, 2] considering the difference lateral stiffness between inner and outer wheels due to load transfer. Through the simulation, it can be obtained that AIFS has better lateral stability than AFS when steering with large lateral acceleration. Meanwhile, a rule-based steering angle decision method and a PI controller are proposed, but it is difficult to achieve the optimal front wheel steering angle decision and the robustness is inadequate. But there is no redundant design in its proposed structure. There is a front wheel additional angle decision algorithm based on tire force control allocation,[3] AIFS and AFS can be realized by transforming the weight coefficient matrix, meanwhile, it has been approved that the lateral stability of the vehicle at ultimate steering through the simulation. A based on the Ackerman steering theorem and considering the front wheel side-slip, the relationship between the tire side-slip angle and the vehicle speed, yaw rate and wheel steering angle is obtained by using the linear 2-DOF vehicle model.[4] The obtained tire side-slip angle is used to modify the steering angle, and the steering angle decision algorithm suitable for front wheel independent steering and four-wheel independent steering is derived. There is a multi-mode steer-by-wire system for emergency rescue vehicles.[5] By setting a hydraulic steering actuator at the wheel sid, the controller controls the state of different solenoid valves to achieve independent control of four steering actuators of vehicle. Hyundai Motor Company design a left and right wheel independent steer-by-wire system.[6] Redundancy is achieved by adding a mechanical steering device, and its redundancy design remains to be studied.

At the same time, for the distributed independent steering system that can achieve even the four-wheel independent steering, it is difficult to achieve mutual redundancy between wheels like distributed braking and driving, which increases the difficulty of redundant design and functional safety. The failure of a single system has a greater impact on the stability and safety of the vehicle. Therefore, a multi-mode steer-by-wire system with high

safety structure of traditional steer-by-wire mechanism and independent control of front wheel steering angle to realize side-slip angle control in active safety chassis are proposed in this paper.

2. STRUCTURE AND MODELING OF THE MULTI-MODE STEER-BY-WIRE SYSTEM

By comparing and analyzing the existing steer-by-wire system, an electric multi-mode steer-by-wire system is proposed, as shown in FIG. 1. The steering actuator of the system is driven by two electric motors, which can not only realize the independent steering of the front wheels, when the electro-valves (Part 4 and 5) are open, but drive the front wheels to steer as the traditional steer-by-wire does which is constrained by the steering trapezium, by closing the electro-valves when one of the motors fails. In the worst case, when both motors fail, the Column-EPS mode can be realized using the retained connection between the steering wheel and the rack. Therefore, the structural redundancy and functional safety of the proposed steer-by-wire system can be improved.

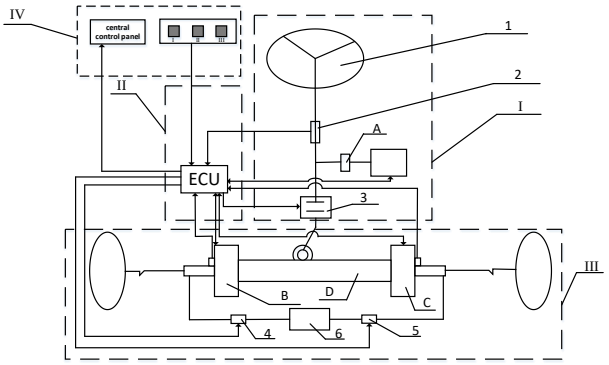

Fig. 1 Structure block diagram of electric multi-mode steer-by-wire

In FIG. 1, I is the steering hand wheel unit including steering hand wheel (1), electromagnetic clutch (3), road-feeling imitation motor (1), torque and angle sensor of the steering hand wheel (2) and reducer (A); III is the steering actuator unit which mainly include steering gear (D), two steering electric motors (B and C), two electro-valves (4 and 5) and oil tank (6). The two steering motors is controlled to implement the active movement of the steering road wheel; II is the electronic control unit which mainly receives the feedback signal from actuators and sensors, meanwhile sends the control signal to the actuators, such as the steering electric motors, road-feeling imitation motor, electromagnetic clutch and two electro-valves; IV is the interface between driver and vehicle for mode selection and status display.

The mechanical structure diagram of the steering actuator proposed in this paper and the simplified dynamic model based on this structure are shown in FIG. 2. From the FIG. 2(a), it can be seen that the steering actuator is composed of motor shell (4, 5), motor stator (3, 6) and motor rotor (2, 7) which connect with guide screw (1, 8) via the ball screw unit. In order to establish its mathematical model, simplify the mechanical structure of the steering actuator into a dynamic model as shown in FIG. 2(b).

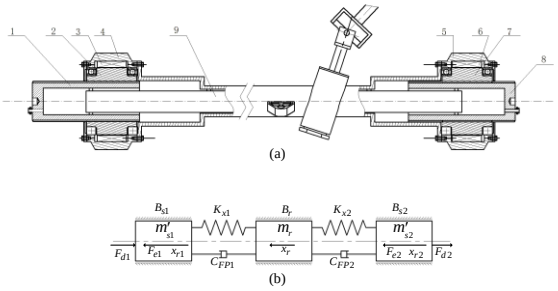

Fig. 2 Steering actuator model proposed in this paper: (a) is the mechanical structure diagram, (b) is the dynamic model

Based on simplified dynamic model, the equation of the front wheel steering actuator is summarized below:

$$\begin{cases} \ddot{x}_{r2}\cdot m_{s2}{}' + \dot{x}_{r2}\cdot B_{s2} = F_{e2} - F_{d2} - k_{m1}\cdot\left(x_{r2}-x_r\right)\cdot K_{x2} - k_{m2}\cdot C_{FP2} \\ \ddot{x}_r\cdot m_r = \left(x_{r2}-x_r\right)\cdot K_{x2} - B_r\cdot\dot{x}_r + \left(x_{r1}-x_r\right)\cdot K_{x1} \\ \ddot{x}_{r1}\cdot m_{s1}{}' + \dot{x}_{r1}\cdot B_{s1} = F_{e1} - F_{d1} - k_{m1}\cdot\left(x_{r1}-x_r\right)\cdot K_{x1} - k_{m2}\cdot C_{FP1} \end{cases} \quad (1)$$

In equation (1), the subscript 1 and 2 in the symbol represent the left and right side, respectively. Where m'_s is the equivalent mass of motor rotor and guide screw and m_r is the mass of the rack (9 in FIG. 2). x_{r1}, x_{r2}, x_r are the displacement of guide screw of left, guide screw of right and rack, respectively. And then K_x is the elastic stiffness of hydraulic camber when the electro-values are closed, C_{FP} is the damping force of the electro-value port when the electro-values are opened and the B_s, B_r are the friction damping. Meanwhile, F_e is the driving force converted by the motor torque through the ball screw unit, F_d is the resistance converted from the steering resistance torque generated by the road. Besides k_{m1}, k_{m2} are the model switching parameters, when the $k_{m1}=0, k_{m2}=1$, the steering actuator dynamic model is represent the independent steering of two front wheels, and when the $k_{m1}=1, k_{m2}=0$, the steering actuator dynamic model is represent the steering of two front wheels constrained by the steering trapezium.

3. PRINCIPLE ANALYSIS AND CONTROL STRATEGY SIMULATION OF ACTIVE SIDE-SLIP CONTROL

3.1. Principle analysis of the active side-slip control

As we know, the force characteristics of the front wheel during cornering are shown in the FIG. 3. The lateral acceleration of the

vehicle body results in the normal load transfer from the inner wheel to the outer wheel, which causes the side-slip stiffness of the two wheels changed. The outer one is generally increase, and the inner one may decrease meanwhile. If the changes can be utilized by independent steering of the two-side steering road wheel, the limit cornering ability of the vehicle can be improved through additional steering angle control of two-side wheels. Therefore, the front wheel steering angles are modified based on the tire side-slip stiffness, then the side-slip angles of two-side wheels also changed, which is generally called active side-slip angle control. This method can make the inner and outer wheels are not in the lateral saturation area of the tire, further utilize the tire adhesion condition to improve the cornering maneuverability and stability, especially in severe turning condition with large lateral acceleration.

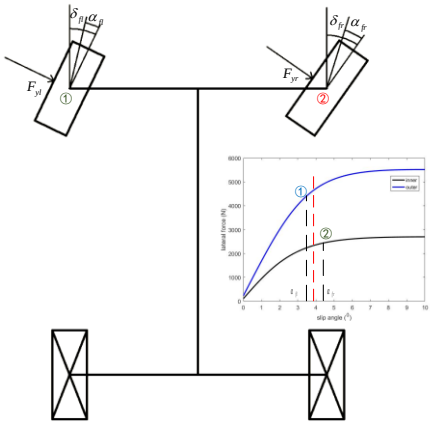

Fig. 3 Force characteristic analysis of front tire

3.2. The active side-slip control strategy

The vehicle simulation architecture based on Simulink and Carsim is shown in FIG. 4, mainly comprised of stability control, angle decision control and steering execution control. Next, the control logic is illustrated via the FIG. 4.

Firstly, the stability control unit based on the sliding model control via the front wheel steering angle that from the variable transmission ratio module (VGRS) and vehicle state especially the yaw rate that from the state identification module can obtain the additional yaw moment which could make the vehicle fellow the desired yaw rate from the reference model. Secondly, the angle distribution controller can obtain the modified front wheel steering angle, through the front wheel steering angle from the VGRS and addition yaw moment from stability control unit. By the way, the model switch unit determines which steering angle decision module is selected, as does the angle actuator in the steering execution unit. Thirdly, the steering execution unit that consists the angle controller and angle actuator receives the modified front wheel steering angle and obtain the real front wheel steering angles, and finally input into the vehicle model based on Carsim.

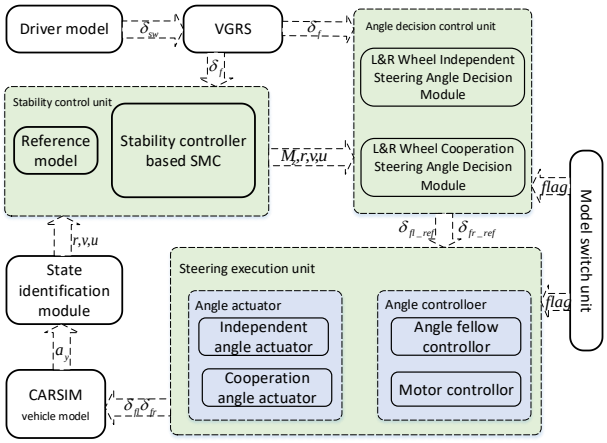

Fig. 4 Vehicle simulation control block diagram

3.2.1. Establishment of stability control unit

In order to make the vehicle maintain the linearity of the steering as much as possible. Therefore, the ideal yaw rate is established by the 2-DOF vehicle model, and then the additional yaw moment output by the stability controller is obtained. Through the angle decision controller, the input front wheel angle is corrected and finally input into the vehicle model, so that the yaw rate of the vehicle follows the ideal yaw rate.

By establishing a linear 2-DOF vehicle model and considering the adhesion condition of the road surface, the reference yaw rate model is shown in equation (2).[7, 8]

$$\omega_{rd} = \min\left\{\left|\frac{v_x\delta_f}{L\left(1+Kv_x^{\ 2}\right)}\right|, \left|\zeta\frac{\mu g}{v_x}\right|\right\} sign\left(\delta_f\right) \tag{2}$$

Where ζ is the correction factor considering the influence of $\dot{v}_y/v_x$ and a_x, then $\zeta = 0.8$.

In order to obtain the additional yaw moment, based on the linear 2-DOF model, the additional yaw moment is introduced to obtain the extended 2-DOF model, as shown in equation (3):

$$\dot{x} = Ax + E\delta_f + HM_z; x = \left[v_y, \omega_r\right]^T$$
$$A = \begin{bmatrix} \frac{k_f + k_r}{mv_x} & \frac{ak_f - bk_r}{mv_x} - v_x \\ \frac{ak_f - bk_r}{I_z v_x} & \frac{a^2k_f + b^2k_r}{I_z v_x} \end{bmatrix}, E = \begin{bmatrix} \frac{-k_f}{m} \\ \frac{-ak_f}{I_z} \end{bmatrix}, H = \begin{bmatrix} 0 \\ \frac{1}{I_z} \end{bmatrix} \tag{3}$$

The error is defined as the difference between the actual yaw rate and the ideal yaw rate, $e = \omega_r - \omega_{rd}$. Select the sliding mode switching function as:

$$s = e + \lambda\int_0^t e(\tau)d\tau \tag{4}$$

Considering the exponential reaching law:

$$\dot{s} = -\varepsilon \operatorname{sgn} s - Ks \quad (5)$$

Where, $\varepsilon > 0, K > 0$. Finally, the control output of the additional yaw moment is:

$$M_z = \left(-\varepsilon \operatorname{sgn} s - Ks + \dot{\omega}_{rd} - \lambda\left(\omega_r - \omega_{rd}\right)\right) I_z - \frac{ak_f - bk_r}{v_x} v_y - \frac{a^2 k_f + b^2 k_r}{v_x} \omega_r + ak_f \delta_f \quad (6)$$

In order to reduce the chattering of the sliding mode controller, the switching function $\operatorname{sgn}(s)$ is the cause of the chattering, so the function with a linear change region $\operatorname{sat}(s)$ is used instead.

$$\operatorname{sat}(s) = \begin{cases} \operatorname{sgn}(s), |s| > \dfrac{1}{\varepsilon} \\ \dfrac{s}{\varepsilon}, |s| < \dfrac{1}{\varepsilon} \end{cases} \quad (7)$$

Where, ε is the boundary layer thickness.

3.2.2. Angle decision strategy based on control allocation

1) Independent angle decision

Because the two steering actuators of the system work independently and simultaneously to meet the demand of the lateral force, it is a typical overdrive system. For overdrive system, the control allocation method is usually used to assign the upper control objectives to each actuator.

The control objectives of the upper layer are obtained by the vehicle stability controller. The specific composition of the angle decision controller in FIG. 4 is shown in FIG. 5.

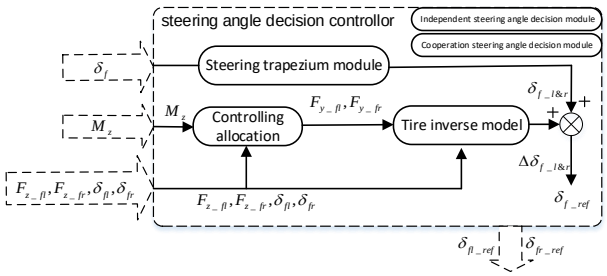

Fig. 5 Steering angle decision controller

The design of the control distributor first considers the relationship between the pseudo control variable and the actual control variable. The pseudo control variable is the upper control target $v = M_z$, and the actual control variable is the additional lateral force of the front wheel $u = \begin{bmatrix} \Delta F_{y\_fl} & \Delta F_{y\_fr} \end{bmatrix}^T$. The relationship is as follows:

$$v = Bu$$

$$B = \begin{bmatrix} a\cos\delta_{fl} + \dfrac{T}{2}\sin\delta_{fl} & a\cos\delta_{fr} - \dfrac{T}{2}\sin\delta_{fr} \end{bmatrix} \quad (8)$$

Then the optimization objective function of the control is characterized, and the tire load is used to represent the control optimization objective, assuming that the longitudinal degree of freedom of the vehicle is not considered, and the longitudinal force on the tire during the steering process is zero, the optimization objective can be simplified to:

$$\min J = \sum_{i=l,r} \frac{\left(F_{yi} + \Delta F_{yi}\right)^2}{\left(\mu F_{zi}\right)^2} \quad (9)$$

Because the tire has the maximum lateral force under the normal load, the constraint of the tire force is used as the constraint condition of the control allocation optimization problem.

$$\begin{cases} F_{yl} + \Delta F_{yl} \le F_{yl\_\max} \\ F_{yr} + \Delta F_{yr} \le F_{yr\_\max} \end{cases} \quad (10)$$

The optimization objectives and constraints are transformed into standard quadratic programming problems:

$$\min J = u^T W_u u \quad s.t. \begin{cases} Bu = v \\ \underline{u} \le u \le \overline{u} \end{cases} \quad (11)$$

The equality constraints $Bu = v$ is transformed into $\min_{\underline{u} \le u \le \overline{u}} \left\| W_v \left(Bu - v \right) \right\|_2$, as part of the optimization objective, the standard quadratic programming problem is transformed into a sequential least squares programming problem (SLS):

$$\begin{cases} u = \arg\min_{u \in \Omega} \left\| W_u \left(u - u_d \right) \right\|_2 \\ \Omega = \arg\min_{\underline{u} \le u \le \overline{u}} \left\| W_v \left(Bu - v \right) \right\|_2 \end{cases} \quad (12)$$

Among $u_d = 0$, it tends to achieve yaw rate tracking with the smallest front wheel tire lateral force output. The weight matrix of the control vector is $W_u = diag\left(1/\left(\mu F_{zl}\right)^2, 1/\left(\mu F_{zr}\right)^2\right)$, and the weight matrix of the distribution demand is W_v , and $W_v = 1$.

Then, by introducing a weight coefficient, the sequential least squares problem is transformed into a weighted least squares problem.[9]

$$u = \arg\min_{\underline{u} \le u \le \overline{u}} \left(\left\| W_u \left(u - u_d \right) \right\|_2^2 + \gamma \left\| W_v \left(Bu - v \right) \right\|_2^2 \right) \quad (13)$$

The formula (13) can be transformed into:

$$\begin{cases} \left\| W_u \left(u - u_d \right) \right\|_2^2 + \gamma \left\| W_v \left(Bu - v \right) \right\|_2^2 == \left\| Au - b \right\|_2^2 \\ A = \begin{bmatrix} \gamma^{\frac{1}{2}} W_v B \\ W_u \end{bmatrix}, b = \begin{bmatrix} \gamma^{\frac{1}{2}} W_v v \\ W_u u_d \end{bmatrix} \end{cases} \quad (14)$$

Therefore, the optimization problem is finally obtained:

$$\begin{cases} \min \left\| Au - b \right\|_2^2 \\ \underline{u} \le u \le \overline{u} \end{cases} \quad (15)$$

In this paper, the active set method (ASM) is used to solve this problem.(10)

2) Cooperation angle decision

Because the tire is in the linear region and the lateral force is not saturated in the case of cooperation steering, the additional lateral force of the front axle can be simply calculated by the additional yaw moment, and then the corresponding additional front wheel angle can be obtained based on the tire inverse model. Finally, the target additional yaw moment control is realized to complete the control of vehicle stability.

3.3. The simulation of active side-slip control

When the vehicle speed is 50 km/h and the road adhesion coefficient is 0.85, the double lane change condition simulation is carried out for the vehicle in mode one and mode three respectively. The trajectory tracking is shown in FIG. 6(a), and the yaw rate tracking curve is shown in FIG. 6(b).

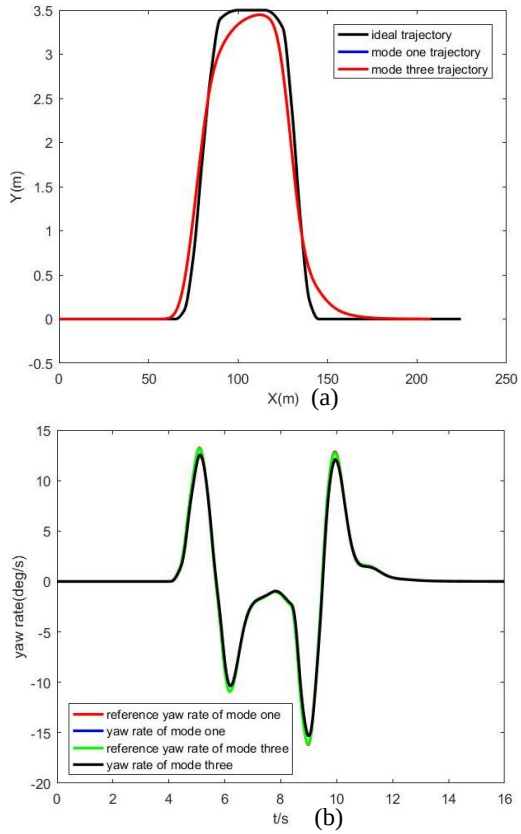

Fig. 6 simulation result of low-speed double lane change: (a) is trajectory tracking curve, (b) is yaw rate curve

From FIG. 6, it can be seen that under low-speed condition, whether the vehicle steering actuator is in mode one or mode three, its trajectory tracking ability and vehicle stability are basically the same. It can be concluded that under low-speed non-limit condition, mode one can not only ensure the tracking ability of the vehicle and the stability of the vehicle, but also reduce the load of steering actuator.

When the vehicle speed is 100 km/h and the road adhesion coefficient is 0.85, the double lane change condition simulation is carried out for the vehicle in mode one and mode three respectively. The trajectory tracking is shown in FIG 7(a), the yaw rate tracking curve is shown in FIG 7(b), and the normalized side-slip stiffness curve is shown in FIG 7(c).

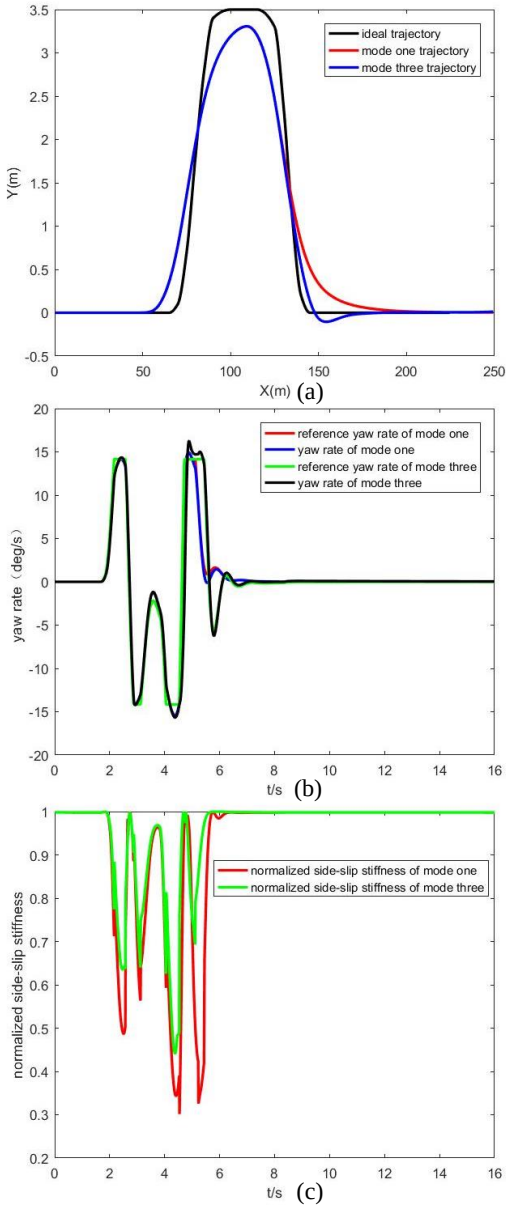

Fig. 7 simulation result of high-speed double lane change: (a) is trajectory tracking curve, (b) is yaw rate curve, (c) is normalized side-slip stiffness curve

From FIG 7(a), it can be seen that the vehicle with mode three has stronger trajectory following ability under high-speed condition. From FIG 7(b), it can be seen that the vehicle with mode one has smaller normalized lateral stiffness of the front wheels due to the saturation of the lateral force of the inner wheels, which cannot provide more lateral force, resulting in larger trajectory

following error. At the same time, it can be seen from FIG 7(b) that the vehicle with mode three can generate greater yaw rate to cope with extreme condition.

When the vehicle speed is 55 km/h and the road adhesion coefficient is 0.85, the steady circular condition simulation is carried out for the steering actuator of the vehicle in mode one and mode three respectively. The trajectory tracking is shown in FIG 8(a), the yaw rate tracking curve is shown in FIG 8(b), and the normalized side-slip stiffness curve is shown in FIG 8(c).

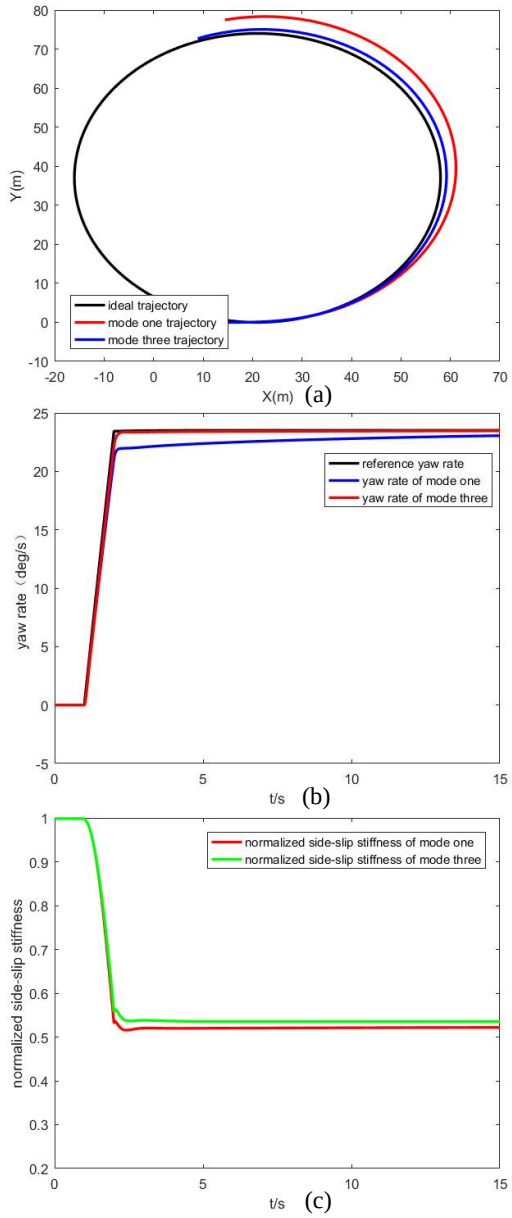

Fig. 8 simulation result of steady circular condition: (a) is trajectory tracking curve, (b) is yaw rate curve, (c) is normalized side-slip stiffness curve

It can be seen from FIG 8(a) that the vehicle using mode three can better follow the target trajectory. It can be seen from FIG 8(b) and FIG 8(c) that the normalized side-slip stiffness of the front wheels on using mode one for steering is smaller. The purpose of yaw stability control can be achieved by reasonable distribution of lateral forces on the left and right wheels without increasing tire load.

4. MODE SWITCHING STRATEGY DESIGN

In the 3 section, the steering angle decision strategy under different steering mode is expounded. In order to apply different steering modes to the actual driving situation, it is necessary to select and switch modes for different vehicle and tire states.

Because the side-slip stiffness of the tire can directly show the side-slip characteristics of the tire, and the tire is in direct contact with the ground when the vehicle is moving, the side-slip characteristics of the tire more directly affect the handling stability of the vehicle. In order to solve the problems caused by the different side-slip characteristics of inner and outer wheels. This paper uses the normalized tire side-slip stiffness as the basis for mode switching.

4.1. Mode switching strategy analysis

Firstly, the normalized tire side-slip stiffness of the inner and outer front wheels are calculated by the normalized tire side-slip stiffness calculation formula,[11, 12] and then the minimum value is taken as the normalized tire side-slip stiffness q judged by the system, as shown in equation (16):

$$q = \min\left(\frac{k_{fl}}{k_{fl0}}, \frac{k_{fr}}{k_{fr0}}\right) \tag{16}$$

Where k_{fl} and k_{fr} are the instantaneous side-slip stiffness of the left and right front wheels, k_{fl0} and k_{fr0} are the linear side-slip stiffness of the left and right front wheels, respectively.

Because the state of the vehicle changes at any time, and the force state of the wheel is improved before and after the mode switching, the q will increase in a short time after the mode switching. If the mode switching is determined by a single side-slip stiffness threshold, the system will be in the process of switching mode switching for a long time, resulting in system chattering and instability, which not only fails to achieve the expected effect, but also may cause damage to the motor and the switching solenoid valve for mode switching.

Based on the above analysis, consider setting a double threshold, which is setting the upper limit $q_{\max}$ of the threshold and the lower limit $q_{\min}$ of the threshold. When q is greater than $q_{\max}$, mode switch from mode one to mode two. When q is less than $q_{\min}$, mode switch from mode two to mode one. The following analysis will be combined with FIG 9. It shows the normalized side-slip

stiffness curve and the mode switching signal curve of the tire under typical double lane change condition.

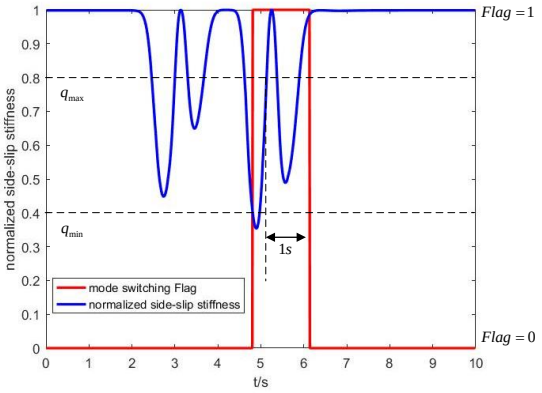

Fig. 9 Schematic diagram of mode switching

From the diagram, it can be seen that when the q is lower than $q_{\min}$, the mode switching signal Flag is 1, and the system switch the mode from one to three to improve the stability of the vehicle. When the q is higher than $q_{\max}$, the system should enter the mode switching from mode three to mode one. However, due to the rapid change of the q, in order to prevent the system mode switching too frequently, when switching from mode three to mode one, the mode switching signal is delayed by one second to trigger, as shown in FIG 9.

4.2. Mode switching strategy simulation

In order to verify the effectiveness of the mode switching strategy and the effectiveness of the yaw stability control when the front wheel lateral force is saturated during the steering process of the vehicle. The steering wheel angle input shown in FIG 10 is used. The simulation analysis is carried out under the condition of 60 km/h speed and 0.85 road adhesion coefficient. FIG 11(a) is the yaw rate following curve in different modes, and FIG 11(b) is the normalized side-slip stiffness curve.

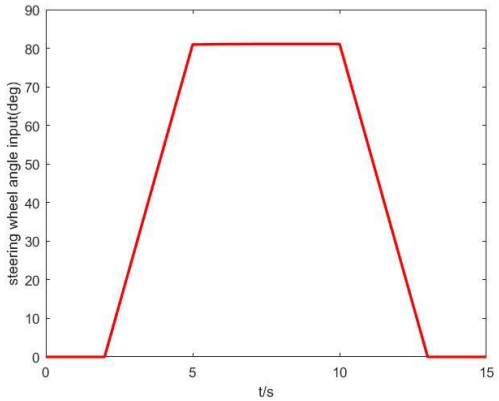

Fig. 10 Steering wheel angle input curve

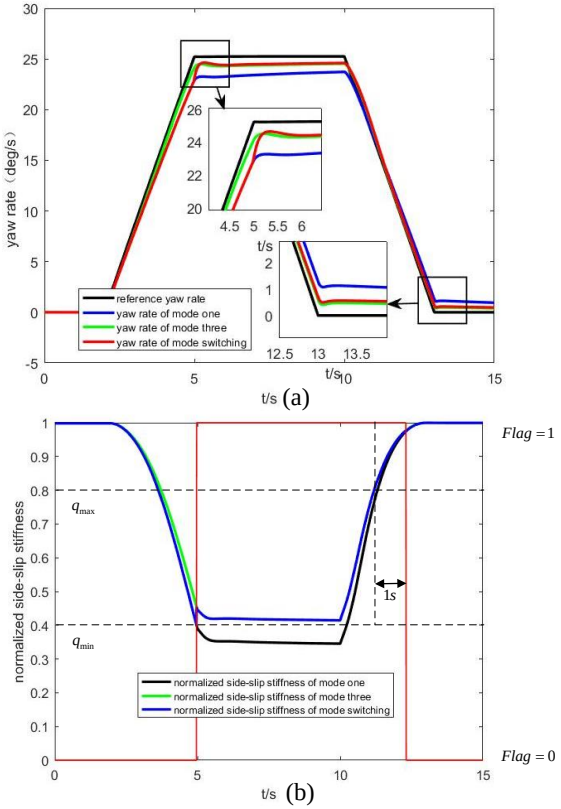

Fig. 11 simulation result of mode switching condition: (a) is yaw rate curve, (b) is normalized side-slip stiffness curve

As shown in FIG 11, the yaw rate following and the optimization of the normalized side-slip stiffness under different modes are compared. It can be seen that the introduction of the mode switching strategy can make the vehicle use mode one to steering under non-limit steering condition. At about the 5 seconds of the simulation, when the normalized side-slip stiffness is lower than $q_{\min}$ the mode switching is carried out. It can be seen that the yaw rate quickly keeps up with the ideal value, and the yaw rate of the vehicle is better followed while improving the normalized side-slip stiffness of the tire, so as to achieve the steering ability of the vehicle in mode three. At the same time, when the normalized side-slip stiffness is higher than $q_{\max}$, delay 1 second, the steering actuator is switched from mode three to mode one, which reduces the load of the steering actuator and reduces the frequency of mode switching.

5. CONCLUSION

In this paper, the feasibility of front wheel independent steering to improve vehicle handling stability was discussed emphatically, and a steer-by-wire actuator system with both centralize steering function and independent steering function was proposed. Then the dynamic model of the proposed multi-mode steer-by-wire system was established. Meanwhile the corresponding integrated

steering angle decision strategy was described. The joint simulation of Simulink and Carsim was carried out to verify the effect of front wheel independent steering on vehicle handling stability. For the traditional steer-by-wire with steering trapezoid constraint, the comparing simulation results showed that the proposed front wheel independent steering system can effectively enhance the tire utilization rate, and improve the vehicle stability margin. Finally, aiming at the mode switching problem of multi-mode steer-by-wire actuator system, the design of mode switching control strategy for multi-mode steer-by-wire actuator is completed by considering the normalized side-slip stiffness of tire. Through the simulation analysis results, it can be seen that the mode switching control strategy can make the vehicle use mode one to steering when the vehicle is under non-limit condition, and use mode three to steering when it is close to reaching the tire adhesion limit. At the same time, a reasonable mode switching control strategy also reduces the frequency of mode switching and ensures the stability of the system.

ACKNOWLEDGMENT

This work was supported in part by the National Natural Science Foundation of China (Grant No. 52272365) and the Jilin Province Science and Technology Major Project (Grant No. 20210301023GX), Jilin Province Natural Science Foundation (Grant No. 20220101200JC), as well as Jilin Province Young and Middle-aged Science and Technology Innovation and Entrepreneurship Excellence Talent (Team) Project (Innovation) (Grant No.20230508050RC).

REFERENCES

(1) Ahmed W, Rawat V, and Bhat R B, “Steering System and Method for Independent Steering of Wheels,” *US, 8126612B2[P]*, February 28, 2012.

(2) Azadeh F, Ahmed A, and Rakheja S, “Performance Enhancement of Road Vehicles Using Active Independent Front Steering (AIFS),” *SAE International Journal of Passenger Cars- Mechanical Systems*, vol. 5, no. 4, pp. 1273-1284, September 2012.

(3) Yuan X W, Wen G L, and Zhou Bing, “Road Wheel Angle Distribution Algorithm for Road Vehicles with AIFS Based on Control Allocation,” *China Mechanical Engineering*, vol. 26, no. 9, pp. 1243-1250, September 2015.

(4) Zong C F, Sun H, Chen G Y, “Steering Angle Allocation Method for Distributed Independent Steering Vehicles,” *Journal of South China University of Technology (Natural Science Edition)*, vol. 45, no. 2, pp. 16-22, February 2017.

(5) Xu F X, Liu X H, and Chen W, “Fractional Order PID Control for Steer-by-Wire System of Emergency Rescue Vehicle Based on Genetic Algorithm,” *Journal of Central South University*, vol. 26, no, 9, pp. 2340-2353, October 2019.

(6) Park S, Hwang S, and Oh Y, “Development of the Independent-Type Steer by Wire System,” *SAE Technical Paper Series*, 2007-01-1148, April 2007.

(7) Zhao W Z, Wang C Y, and Sun P K, “Primary Studies on Integration Optimization of Differential Steering of Electric Vehicle with Motorized Wheels Based on Quality Engineering,” *Science China Technological Sciences*, vol. 54, no. 11, pp. 3047-3053, November 2011.

(8) Li, D F, Du S Q, and Yu F, "Integrated Vehicle Chassis Control Based on Direct Yaw Moment, Active Steering and Active Stabiliser," *Vehicle System Dynamics*, vol. 46, no. sup1, pp. 341-351, January 2008.

(9) Gao W B, *Theory and Design Method of Variable Structure Control*, Science Press, 1996.

(10) Chen B L, *Optimization Theory and Algorithms*, Tsinghua University Press, 2005.

(11) Zhong Z N, Zhao E J, and Zheng X, “A Consensus-Based Square-Root Cubature Kalman Filter for Manoeuvring Target Tracking in Sensor Networks,” *Transactions of the Institute of Measurement and Control*, vol. 42, no. 1, pp. 3052-3062, July 2020.

(12) Viehweider A, and Hori Y, “Electric Vehicle Lateral Dynamics Control Based on Instantaneous Cornering Stiffness Estimation and an Efficient Allocation Scheme,” *IFAC Proceedings Volumes*, vol. 45, no. 2, pp. 1213-1218, March 2012.